High-spin states in ^{133}Cs and the shell model description

S. Biswas, R. Palit, J. Sethi, S. Saha, A. Raghav, U. Garg, Md. S. R. Laskar, F. S. Babra, Z. Naik, S. Sharma, A. Y. Deo, V. V. Parkar, B. S. Naidu, R. Donthi, S. Jadhav, H. C. Jain, P. K. Joshi, S. Sihotra, S. Kumar, D. Mehta, G. Mukherjee, A. Goswami, and P. C. Srivastava

High-spin states in ^{133}Cs and the shell model description

S. Biswas[1], R. Palit[1],* J. Sethi[1], S. Saha[1], A. Raghav[2], U. Garg[3], Md. S. R. Laskar[1], F. S. Babra[1],
Z. Naik[1], S. Sharma[1], A. Y. Deo[1,4], V. V. Parkar[1,5], B. S. Naidu[1], R. Donthi[1], S. Jadhav[1], H. C. Jain[1],
P. K. Joshi[6], S. Sihotra[7], S. Kumar[8], D. Mehta[7], G. Mukherjee[9,10], A. Goswami[11], and P. C. Srivastava[4]

[1]*Department of Nuclear and Atomic Physics, Tata Institute of Fundamental Research, Mumbai 400005, India*
[2]*Department of Physics, University of Mumbai, Mumbai 400098, India*
[3]*University of Notre Dame, Indiana 46556, USA*
[4]*Department of Physics, Indian Institute of Technology, Roorkee 247667, India*
[5]*Bhabha Atomic Research Centre, Mumbai 400085, India*
[6]*HBCSE, Tata Institute of Fundamental Research, Mumbai 400088, India*
[7]*Department of Physics, Panjab University, Chandigarh, India*
[8]*Department of Physics, Delhi University, New Delhi, India*
[9]*Physics Group, Variable Energy Cyclotron Centre, 1/AF Bidhan Nagar, Kolkata 700064, India*
[10]*Homi Bhabha National Institute, Training School Complex, Anushaktinagar, Mumbai 400094, India and*
[11]*Nuclear Physics Division, Saha Institute of Nuclear Physics, Kolkata 700064, India*
(Dated: May 25, 2017)

The high-spin states in ^{133}Cs, populated using the reaction ^{130}Te(^{7}Li,4n) with 45 MeV beam energy, have been extended up to an excitation energy of 5.265 MeV using the Indian National Gamma Array (INGA). The observed one- and three-quasiparticle bands in ^{133}Cs, built on the $\pi h_{11/2}, \pi g_{7/2}, \pi d_{5/2}$; and $(\pi g_{7/2} \pi d_{5/2})^1 \otimes \nu h_{11/2}^{-2}$ configurations, respectively, have similar structure as seen in the lighter odd-A Cs isotopes. The experimental level scheme has been compared with the large scale shell model calculation without truncation using the $jj55pna$ interaction, showing a good agreement for both positive and negative-parity states.

I. INTRODUCTION

The study of high-spin states of Cs isotopes with proton particles beyond $Z = 50$ and neutron holes below $N = 82$ continues to provide information on variety of nuclear structure phenomena like signature inversion [1], chirality [2], etc. The heavier Cs isotopes near the $N = 82$ closed shell are the testing ground of continuously evolving shell model calculations based on the effective interactions [3, 4]. With the increasing neutron number, the Finite-Range Liquid-Drop Model (FRLDM) predicts an evolution of ground state shape from deformed to spherical, while going from ^{121}Cs to ^{137}Cs [5]. Here, the active orbitals for the neutrons are $h_{11/2}$, $s_{1/2}$ and $d_{3/2}$, and that of protons are $h_{11/2}$, $g_{7/2}$, $d_{5/2}$ and $g_{9/2}$. Cesium isotopes are the best examples in this mass region which show four distinct one-quasiparticle collective features [6–11]; (i) a series of $\Delta I = 2$ bands built on $11/2^-$ state in $^{119-131}$Cs, (ii) a series of $\Delta I = 2$ bands built on $7/2^+$ state in $^{125-133}$Cs, (iii) a series of $\Delta I = 2$ bands built on $5/2^+$ state in $^{129-131}$Cs, and (iv) a series of $\Delta I = 1$ bands built on $9/2^+$ state in $^{119-127}$Cs. The ^{135}Cs isotope, being very close to the shell closure has a spherical structure and shell model calculations compare favorably with the observed level scheme [3].

In a recent shell model calculation [4], excited states of ^{131,133,135,137}Cs isotopes were studied and compared with the experimental states. While the calculation provided an overall good description of the excited positive-parity medium-spin states, discrepancies between theory

and experiment have been noted for the relative ordering of low-spin positive-parity states. In this calculation, as the two-body interactions which affect the negative-parity states have not been introduced, large inconsistencies for the negative-parity states have been observed. The calculation also pointed out its limitation in explaining the states associated with neutron and proton interaction.

The ^{133}Cs isotope lies in between the deformed ^{131}Cs and the spherical ^{135}Cs, and is the subject of present investigation. Previously, the low-lying excited states in ^{133}Cs were studied via the reaction ^{130}Te(α,n)^{133}Xe which in turn β-decays to ^{133}Cs [12], and from the decay of ^{133}Ba [13]. The high-spin states of ^{133}Cs were populated up to an excitation energy of 2.833 MeV using the reaction ^{130}Te(^{6}Li,3n)^{133}Cs [11]. In the present work, the high-spin states were investigated using the reaction ^{130}Te(^{7}Li,4n)^{133}Cs up to an excitation energy of 5.265 MeV. An extension of the available level structure of ^{133}Cs up to high spin for both positive and negative-parity states was required to see how its high spin states compare with that of the lighter odd-A Cs isotopes which have regular band structures as well as the heavier isotopes, i.e., ^{135,137}Cs, which show shell model like excitation. These chain of nuclei would provide good testing ground for various theoretical models. In the present manuscript, we have restricted to the comparison with the large scale shell model (LSSM) calculations without truncation, which is possible up to ^{133}Cs isotope below $N = 82$. The comparison of the measured level structure up to high spin for ^{133}Cs with large scale shell model calculation without truncation will test the effective interaction used in the shell model calculation and provide
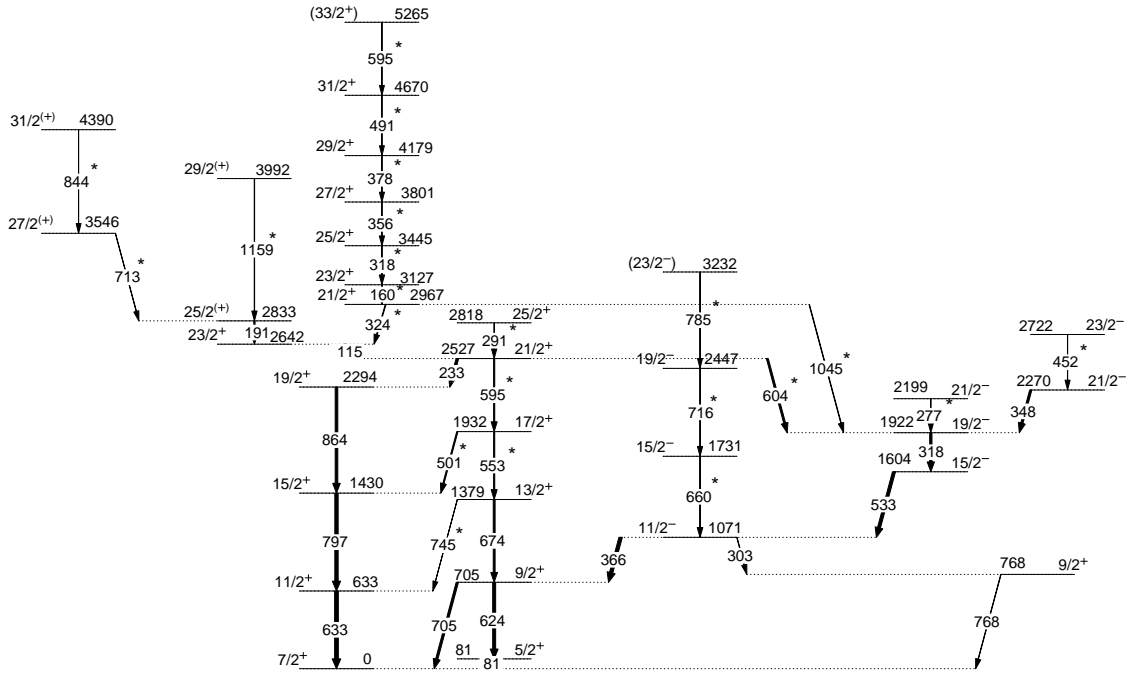
FIG. 1. Level scheme of ^{133}Cs. Transitions marked with an asterisk are new.

a guidance for the interpretation of the excited states.

The current paper is organized as follows: The experimental details are given in the Section II. Section III discusses the experimental results. Section IV shows the systematics of Cs isotopes, and comparison between the experimental observations and theoretical calculations with Large Scale Shell Model (LSSM). Section V briefly summarizes the work reported in the paper.

II. EXPERIMENTAL DETAILS

The experiment was carried out with the Indian National Gamma Array (INGA) at Tata Institute of Fundamental Research (TIFR), Mumbai using the reaction ^{130}Te(^{7}Li,4n)^{133}Cs. A ^{7}Li beam with 45 MeV energy was bombarded on a 5-mg/cm^2 ^{130}Te target backed with 2-mg/cm^2 Al. During the experiment, there were 15 Compton Suppressed High Purity Germanium (HPGe) clover detectors in the array. The detectors

were placed in rings at angles (number of detectors) $40°(2), 65°(2), 115°(2), 140°(2), 157°(3)$ and $90°(4)$ with respect to the beam direction. Gamma-rays emitted from the deexciting residual nuclei were detected in the array and stored with a Digital Data AcQuisition (DDAQ) system, based on Pixie-16 modules of XIA LLC [14], in two-fold coincidence mode.

The time stamped data were processed on an event by event basis into γ-γ matrices and γ-γ-γ cubes for subsequent analysis using the MultipARameter COincidence Search program developed at TIFR [15]. There were about 1.06×10^8 events in the γ-γ-γ cube, which was analyzed using the RADWARE package [16] to obtain the coincidences among the different γ rays to construct the level scheme. The spin of the levels were obtained using Directional Correlation from Oriented states (DCO), using the detectors at 90° and 157°, defined by the following relation [17]:

$$R_{DCO} = \frac{I_{\gamma_1}(\text{measured at } 157°; \text{ gated by } \gamma_2 \text{ at } 90°)}{I_{\gamma_1}(\text{measured at } 90°; \text{ gated by } \gamma_2 \text{ at } 157°)}$$
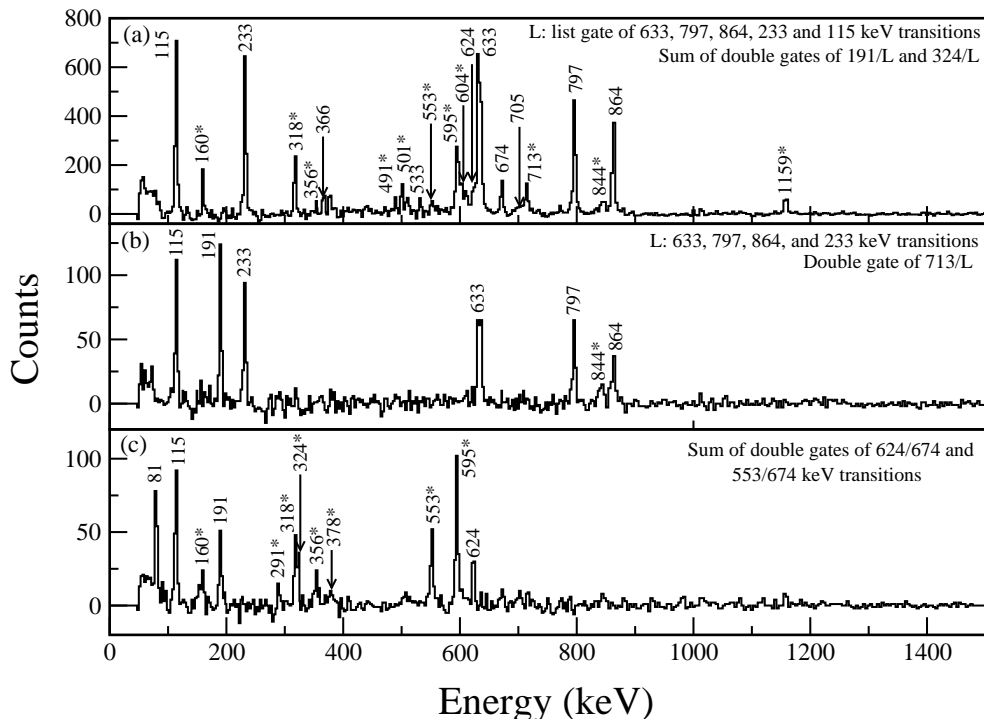
FIG. 2. (a) Spectrum obtained by sum of double gates of 191/L and 324/L keV, L depicting a list gate of 633-, 797-, 864-, 233- and 115-keV transitions. (b) Spectrum obtained by double gating on 713/L with L denoting a list gate of 633-, 797-, 864-, and 233-keV transitions. (c) Spectrum obtained by sum of double gates on 624- and 674-; and 553- and 674-keV transitions. The newly observed transitions have been marked with an asterisk.

The DCO ratios of stretched dipole and quadrupole transitions are ∼0.5(1.0) and ∼1.0(2.0), respectively, for a pure quadrupole (dipole) gate.

The parities of the states were obtained by measuring the polarization asymmetry (Δ) defined as in Ref. [18]:

$$\Delta = \frac{a(E_\gamma)N_\perp - N_\parallel}{a(E_\gamma)N_\perp + N_\parallel}$$

using the clover detectors as a polarimeter, for which all the four 90° detectors were used [19]. Here, $N_\parallel(N_\perp)$ is the number of γ transitions scattered parallel (perpendicular) to the reaction plane and $a(E_\gamma)$ is a correction factor for the parallel to perpendicular scattering asymmetry within the crystals of a clover. In the present experiment, for the four clovers kept at 90° with respect to the beam direction, $a(E_\gamma)$ was measured as 1.00(1) from the ^{133}Ba and ^{152}Eu sources. Using the integrated polarization direction correlation method [18], the polarization asymmetry values of the γ transitions have been extracted. For this analysis, two asymmetric matrices were constructed with coincident events corresponding to parallel or perpendicular scattered γ rays at 90° detectors with another γ ray detected at any other angle. In the case of unmixed stretched transition, a positive (negative) value of the polarization asymmetry indicates the electric (magnetic) nature of the transitions [20].

III. EXPERIMENTAL RESULTS

The level scheme of ^{133}Cs established in this work is shown in Fig. 1. In the present work, 22 new transitions have been identified both in the positive-parity and the negative-parity bands. The new transitions have been marked with an asterisk in Fig. 1. A list of the level energies (E$_i$), γ-ray energies (E$_\gamma$), initial and final spins along with the parities of the levels (I$_i^\pi \rightarrow$ I$_f^\pi$), relative intensities (I$_\gamma$), DCO-Ratio (R_{DCO}), and polarization asymmetry (Δ) values is given in Table I. Multipolarities of most of the transitions are extracted from the stretched ΔI = 2 transitions with 533, 624, 633, 674, and 797 keV energies.

1. Positive-Parity States

In the level scheme of ^{133}Cs reported in Ref. [11], positive-parity states have been observed up to $I^\pi = 19/2^+$ at an excitation energy of 2.295 MeV. Three more transitions extending up to spin (25/2) above the 19/2$^+$ state, were identified in this reference, but the parities of those states had not been identified.

In the present work, the positive-parity band has been extended to $I^\pi = (33/2^+)$ with an excitation energy of 5.265 MeV. A strong $\Delta I = 2$ band, consisting of 633-, 797-, and 864-keV transitions built on the 7/2$^+$ state, has been observed which is consistent with the previ-
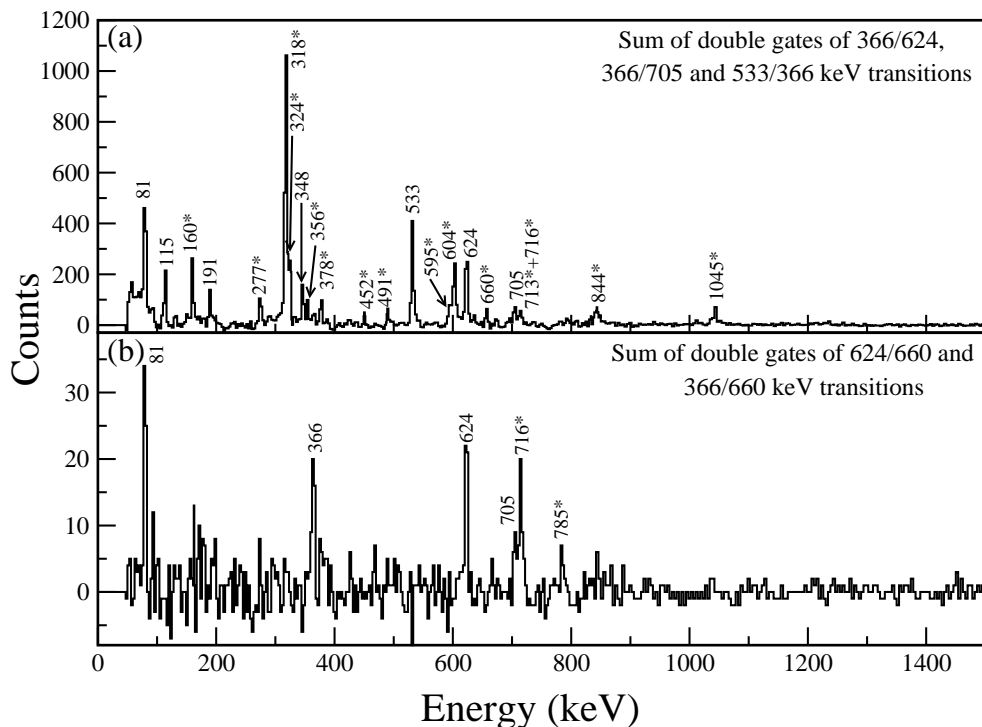
FIG. 3. (a) Spectrum obtained by sum of double gates on 366- and 624-; 366- and 705-; and 533- and 366-keV transitions. (b) Spectrum obtained by sum of double gates on 624- and 660-; 366- and 660-keV transitions.

ous work. The 233-, 115- and 191-keV transitions, which were identified as dipole transitions in the previous work, have also been observed in the present work as evident from the measured values of R_{DCO} in the 633 keV gate. The parity of the 2.527 MeV state, which deexcites by the 233-keV transition was confirmed by the R_{DCO} and Δ values for 604-keV transition. A sum of double gates of 191/L and 324/L with L denoting the list gate of 633-, 797-, 864-, 233- and 115-keV transitions, has been shown in Fig. 2(a). This spectrum shows many of the new transitions, namely the 160, 318, 356, 378, 491, 501, 553, 595, 604, 713, 844 and 1159 keV and have been marked with asterisks. The 501-keV interconnecting transition has a $\Delta I = 1$, M1 character. The other interconnecting transition, namely the 745-keV transition (shown in the level scheme), is not seen in this spectrum as it is very weak, but confirmed in the double gate of 633- and 553-keV transitions. The spin and parity of the 2.967 MeV state, which is populated by the 160-keV transition, is fixed by the 324- and 1045-keV transitions. With the measured R_{DCO} in the 633-keV gate and Δ values , the 318-, 356-, 378-, and 491-keV transitions have been assigned as forming a $\Delta I = 1$ band with M1 transitions. The R_{DCO} of the 160-keV transition in the 633-keV gate suggests $\Delta I = 1$ nature and since it has been observed in coincidence with the 318-, 356-, 378-, 491-, and 595-keV transitions and further assuming its magnetic nature (due to the similarity with the lower-A Cs isotopes), this cascade of $\Delta I = 1$ γ-ray transitions has been designated as a M1 band. The newly identified 1159-keV transition has been assigned as

$\Delta I = 2$, E2 transition from the measured R_{DCO} in the 633-keV gate and Δ value. With a double gate on 713/L with L being the list gate of 633-, 797-, 864-, and 233-keV transitions, a new 844-keV transition is observed in addition to the known 115-, 191-, 233-, 633-, 797-, and 864-keV transitions, as shown in Fig. 2(b). This 844-keV transition has been identified as $\Delta I = 2$, E2 transition.

Another new $\Delta I = 2$ cascade of 624-, 674-, 553-, 595-, and 291-keV γ-rays built on the $5/2^+$ state has been observed in the present work. Though the 624-keV transition was already established in the previous work [11], this 674-keV transition was placed in the negative-parity band in coincidence with the 366- and 624-keV transitions. However with a double gate on 624- and 366-keV transitions, the 674-keV transition has not been observed. Fig. 2(c) shows the spectrum obtained by sum of double gates of 624/674; and 553/674-keV transitions. This spectrum shows the 81-, 115-, 160-, 191-, 291-, 318-, 324-, 356-, 378-, 553- , 595-, and 624-keV coincident transitions. The newly observed 553-, 595- and 291-keV transitions are $\Delta I = 2$ transitions.

2. Negative-Parity States

In the previous work [11], the negative-parity states were reported up to $I^\pi = (15/2^-)$ at an excitation energy of 1.604 MeV. Two more transitions of 318 and 348 keV were identified above this $(15/2^-)$ states in this reference, and the corresponding states with excitation ener-

TABLE I. Level energies (E_i), γ-ray energies (E_γ), initial and final spins and parities of the levels ($I_i^\pi \to I_f^\pi$), relative intensities (I_γ), DCO-Ratio (R_{DCO}), and polarization asymmetry (Δ) values for ^{133}Cs arranged in order of increasing excitation energies. The uncertainties in the energies of γ rays are 0.5 keV for intense peaks and 0.7 keV for weak peaks.

E_i (keV)	E_γ (keV)	$I_i^\pi \to I_f^\pi$	I_γ	DCO-Ratio (R_{DCO})	Polarization Asymmetry (Δ)	Assignment
81	80.8	$5/2^+ \longrightarrow 7/2^+$	318(22)	0.58(9)		M1
633	632.7	$11/2^+ \longrightarrow 7/2^+$	100	1.00(15)	0.112(19)	E2
705	623.9	$9/2^+ \longrightarrow 5/2^+$	96(5)	0.98(14)	0.089(13)	E2
705	705.4	$9/2^+ \longrightarrow 7/2^+$	22(4)	0.53(10)	-0.059(12)	M1
768	767.6	$9/2^+ \longrightarrow 7/2^+$	7.3(7)	0.58(9)	-0.041(27)	M1
1071	303.4	$11/2^- \longrightarrow 9/2^+$	5.6(8)	0.55(9)	0.048(28)	E1
1071	366.3	$11/2^- \longrightarrow 9/2^+$	53(4)	0.61(10)	0.118(33)	E1
1379	674.4	$13/2^+ \longrightarrow 9/2^+$	39(3)	1.03(16)	0.169(25)	E2
1379	745.4	$13/2^+ \longrightarrow 11/2^+$	0.3(1)			M1
1430	796.7	$15/2^+ \longrightarrow 11/2^+$	86(5)	0.96(15)	0.057(13)	E2
1604	533.4	$15/2^- \longrightarrow 11/2^-$	48(4)	1.02(15)	0.084(19)	E2
1731	659.7	$15/2^- \longrightarrow 11/2^-$	9(1)	1.09(25)	0.068(34)	E2
1922	318.2	$19/2^- \longrightarrow 15/2^-$	35(4)	0.95(14)	0.055(12)	E2
1932	501.4	$17/2^+ \longrightarrow 15/2^+$	21(3)	0.46(10)	-0.078(27)	M1
1932	552.6	$17/2^+ \longrightarrow 13/2^+$	18(3)	0.81(13)	0.156(77)	E2
2199	277.2	$21/2^- \longrightarrow 19/2^-$	4.2(8)	0.54(15)	-0.032(13)	M1
2270	347.6	$21/2^- \longrightarrow 19/2^-$	8(2)	0.44(12)	-0.038(13)	M1
2294	864.3	$19/2^+ \longrightarrow 15/2^+$	57(5)	0.95(15)	0.074(12)	E2
2447	715.8	$19/2^- \longrightarrow 15/2^-$	3.1(4)	0.85(11)	0.167(23)	E2
2527	233.0	$21/2^+ \longrightarrow 19/2^+$	39(4)	0.61(10)	-0.086(28)	M1
2527	595.4	$21/2^+ \longrightarrow 17/2^+$	9(2)			E2
2527	604.1	$21/2^+ \longrightarrow 19/2^-$	12(3)	0.62(18)	0.034(17)	E1
2642	114.7	$23/2^+ \longrightarrow 21/2^+$	37(6)	0.62(9)		M1
2722	452.2	$23/2^- \longrightarrow 21/2^-$	2.5(5)	0.54(10)	-0.043(12)	M1
2818	290.7	$25/2^+ \longrightarrow 21/2^+$	4.8(8)	0.93(17)	0.114(42)	E2
2833	190.7	$25/2^{(+)} \longrightarrow 23/2^+$	7.5(9)	0.60(9)		
2967	324.2	$21/2^+ \longrightarrow 23/2^+$	25(5)	0.57(11)	-0.048(15)	M1
2967	1044.7	$21/2^+ \longrightarrow 19/2^-$	5.1(7)	0.59(10)	0.132(70)	E1
3127	160.3	$23/2^+ \longrightarrow 21/2^+$	23(4)	0.51(12)		
3232	785.2	$(23/2^-) \longrightarrow 19/2^-$	0.5(2)			
3445	318.2	$25/2^+ \longrightarrow 23/2^+$	18(3)	0.64(10)	-0.045(24)	M1
3546	713.2	$27/2^{(+)} \longrightarrow 25/2^{(+)}$	2.9(6)	0.50(11)	-0.042(21)	M1
3801	355.6	$27/2^+ \longrightarrow 25/2^+$	12(2)	0.51(10)	-0.127(31)	M1
3992	1158.9	$29/2^{(+)} \longrightarrow 25/2^{(+)}$	2.1(4)	1.06(20)	0.058(23)	E2
4179	377.8	$29/2^+ \longrightarrow 27/2^+$	8.9(9)	0.69(12)	-0.030(15)	M1
4390	844.4	$31/2^{(+)} \longrightarrow 27/2^{(+)}$	2.3(3)	0.89(12)	0.103(35)	E2
4670	490.7	$31/2^+ \longrightarrow 29/2^+$	3.3(5)	0.67(10)	-0.117(33)	M1
5265	595.3	$(33/2^+) \longrightarrow 31/2^+$	0.8(3)			

gies 1.923 and 1.952 MeV were assigned the spins (19/2) and (17/2), respectively, but the parities were not measured.

In the present work, the negative-parity band has been extended up to $I^\pi = (23/2^-)$ with an excitation energy of 3.232 MeV. To obtain the γ-ray transitions at higher spins, a spectrum was obtained by sum of double gates of 366/624; 366/705; and 533/366-keV transitions as depicted in Fig. 3(a). New γ rays 160-, 277-, 318-, 324-, 356-, 378-, 452-, 491-, 595-, 604-, 660-, 713-, 716-, 844- and 1045-keV transitions are observed in coincidence. The 160-, 318-, 324-, 356-, 378-, 491-, 595-, 713- and 844-keV transitions have already been observed in the positive-parity band, with 318-keV being a doublet. Out of the remaining transitions, the measured R_{DCO} in the 624-keV gate and Δ values show that the 604-, and 1045-keV transitions have a $\Delta I = 1$, E1 character. The positive-parity band is connected to the negative-parity states by these two transitions. A newly observed M1 transition, 277 keV, is in coincidence with the 533-, and 366-keV transitions. Also, the 452-keV M1 transition is in coincidence with the 348-keV transition. In addition, 660- and 716-keV E2 transitions have been observed in coincidence too. In order to see higher spin states above the 660- and 716-keV transitions, a spectrum was obtained by sum of double gates of 624/660; and 366/660-keV transitions as
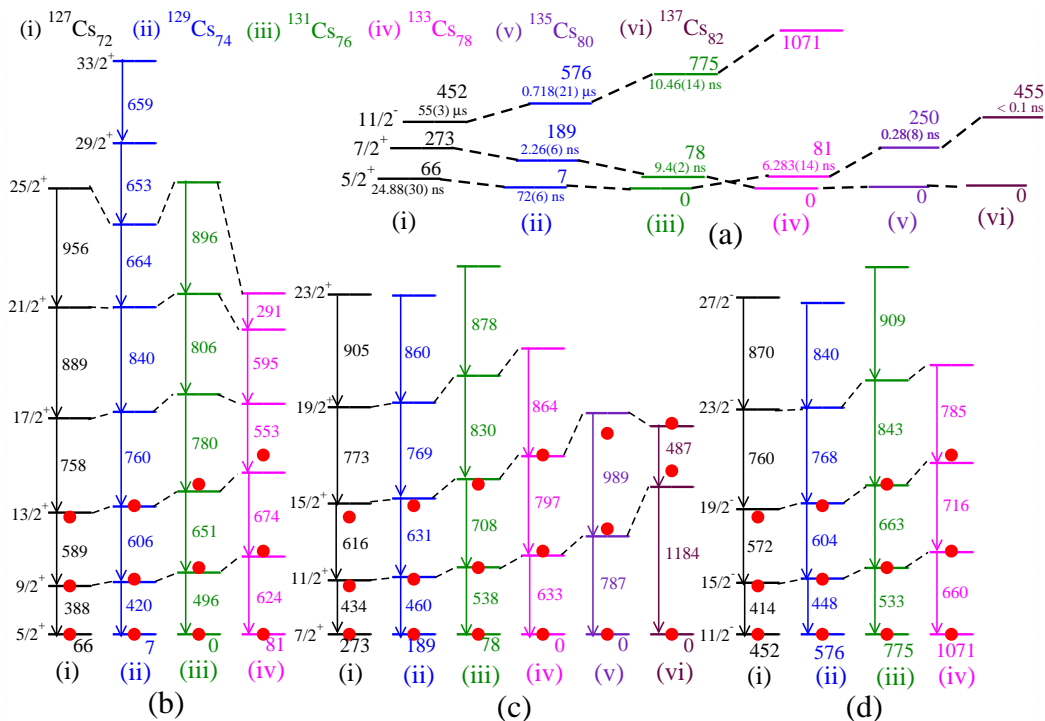
FIG. 4. (Color online) (a) The evolution of the $5/2^+$, $7/2^+$ and $11/2^-$ bandheads as a function of neutron number for the odd-A $^{127-137}$Cs isotopes denoted by indices (i-vi): (i) ^{127}Cs$_{72}$ (black), (ii) ^{129}Cs$_{74}$ (blue), (iii) ^{131}Cs$_{76}$ (green), (iv) ^{133}Cs$_{78}$ (magenta), (v) ^{135}Cs$_{80}$ (indigo) and (vi) ^{137}Cs$_{82}$ (maroon)). The bandhead energies and their half-life (wherever known) has also been quoted. Comparison of the bands built on (b) $5/2^+$, (c) $7/2^+$, and (d) $11/2^-$ states in odd-A $^{127-137}$Cs isotopes [3, 8, 21–23]. The excitation energies corresponding to $J^\pi = 0^+$, 2^+ and 4^+ states of even-A $^{126-136}$Xe isotopes have been shown by red circles.

shown in Fig. 3(b). Newly identified 716-keV E2 transition, and 785-keV transition have been observed in coincidence in this spectrum.

IV. CALCULATIONS AND DISCUSSION

1. Energy Systematics

One- and three-quasiparticle bands similar to those observed in $^{127-131}$Cs [6–11] have also been observed in ^{133}Cs. Three distinct one-quasiparticle band structures have been observed in ^{133}Cs: (i) a $\Delta I = 2$ band built over the $5/2^+$ state (ii) a $\Delta I = 2$ band built over the $7/2^+$ state (iii) a $\Delta I = 2$ band built over the $11/2^-$ state.

The evolution of bandhead energies as a function of neutron number ($N = 72$ (black), 74 (blue), 76 (green), 78 (magenta), 80 (indigo), and 82 (maroon)) corresponding to the isotopes ^{127,129,131,133,135,137}Cs, respectively, has been shown in Fig. 4(a) [3, 8, 21–23]. As can be seen from Fig. 4 (a), there is a decrease in the bandhead energy of the $5/2^+$ state till $N = 76$ and again increases at $N = 78$. Also, the bandhead energy of the $7/2^+$ state decreases as a function of N, in contrary to that for the $11/2^-$ state, showing that the $7/2^+$ band

becomes highly yrast and the $11/2^-$ band becomes non-yrast as N increases from 72 to 78. Systematics of the two positive-parity (built on $5/2^+$ and $7/2^+$ states) and negative-parity (built on $11/2^-$ state) one-quasiparticle band structures in odd-A $^{127-137}$Cs (shown in black, blue, green, magenta, indigo, and maroon colors respectively) have been shown in Figs. 4 (b), (c) and (d), respectively. The relative excitation energies of the excited states of the $5/2^+$ band (Fig. 4 (b)) increases till spin $13/2^+$ with increasing N, but decreases above that in the case of ^{133}Cs showing a structural change of this band in ^{133}Cs. Also, the increase in the relative excitation energies of the $7/2^+$ band with increasing N (Fig. 4 (c)) shows that the deformation decreases as N increases. Again the increase in the relative excitation energies of the $11/2^-$ band with increasing N (Fig. 4 (d)) shows that the deformation decreases from $N = 72$ to 78. These band structures have also been compared with the yrast bands of respective even-even Xe isotopes to probe the evolution of collectivity in odd-Cs. The evolution of the three bands matches quite well with that of the even-even Xe isotopes. This shows that the valance proton occupancy in odd-Cs doesn't have a strong influence on the evolution of deformation of odd-Cs isotopes. The positive-parity three-quasiparticle band structures in odd-A $^{127-133}$Cs have also been studied and they follow the systematics
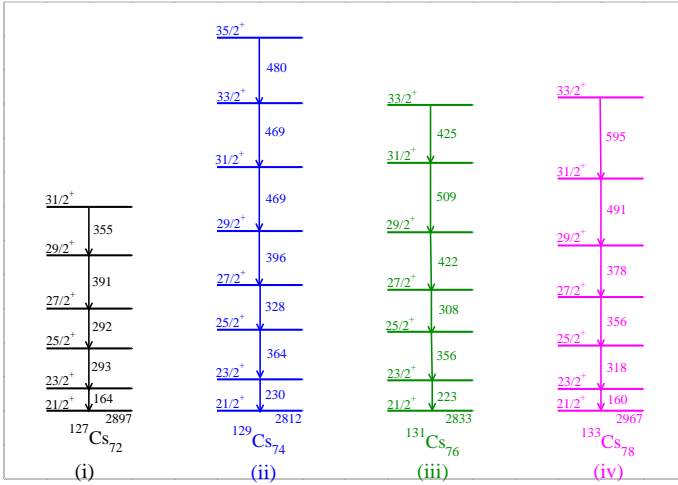
FIG. 5. (Color online) The evolution of the dipole band as a function of neutron number for the odd-A $^{127-133}$Cs isotopes denoted by indices (i-iv): (i) ^{127}Cs$_{72}$ [8] (black), (ii) ^{129}Cs$_{74}$ (blue) [24], (iii) ^{131}Cs$_{76}$ (green) [22], and (iv) ^{133}Cs$_{78}$ (magenta).

as well (see Fig. 5) [8, 22, 24].

2. Large Scale Shell Model (LSSM) Calculations

The wavefunctions for the excited states in ^{133}Cs can be understood microscopically by comparing with the Large Scale Shell Model (LSSM) calculations, carried out using the code NuShellX [25, 26], without any truncation. The orbitals, $0g_{7/2}$, $1d_{5/2}$, $1d_{3/2}$, $2s_{1/2}$ and $0h_{11/2}$ outside of the ^{100}Sn core, were used as the valence space for both protons and neutrons. The single-particle energies used with the $jj55pna$ interaction [27] are 0.80720 $(\pi 0g_{7/2})$, 1.56230 $(\pi 1d_{5/2})$, 3.31600 $(\pi 1d_{3/2})$, 3.22380 $(\pi 2s_{1/2})$, 3.60510 $(\pi 0h_{11/2})$, -10.60890 $(\nu 0g_{7/2})$, -10.28930 $(\nu 1d_{5/2})$, -8.71670 $(\nu 1d_{3/2})$, -8.69440 $(\nu 2s_{1/2})$ and -8.81520 $(\nu 0h_{11/2})$ MeV. The single particle energies of these orbitals were chosen so as to reproduce the excited states in ^{133}Sb and ^{131}Sn. The residual two-body matrix elements for the $jj55pna$ interaction was obtained starting with a G matrix derived from the CD-Bonn nucleon-nucleon potential [28]. The n-n interaction strength for the $jj55pna$ interaction was reduced by a factor of 0.9 to better reproduce the levels in ^{130}Sn [27]. This interaction has been used to explain the excited states in $^{119-126}$Sn [29, 30], $^{124-132}$Te [31, 32], and $N = 82$ isotones ^{136}Xe, ^{137}Cs, ^{138}Ba, ^{139}La, and ^{140}Ce [33].

The Fig. 6 above shows a comparison of the experimentally obtained positive-parity yrast, dipole, and negative-parity bands with those obtained from shell model calculations. Previously in Ref. [4], the same model space was used but with the inclusion of an extended pairing plus quadrupole-quadrupole effective interaction to calculate the excited states of Sn, Sb, Te, I, Xe, Cs and Ba isotopes.

In the case of ^{133}Cs, the ordering of $7/2^+$ and $5/2^+$ states were reversed. Also, they did not obtain good agreement for the negative-parity states. It is evident from this figure that the shell model predicts quite well the positive- and negative-parity E2 bands within ~ 150 keV for most spins, but ~ 350 keV for the $21/2_1^+ - 25/2_1^+$ states. However it underestimates the energies of the dipole band by ~ 800 keV. There are a few features which are well reproduced in the calculations and are thus worth mentioning: (i) the ordering of the $7/2^+$ and $5/2^+$ states is correctly predicted with the energy difference being 4 keV, (ii) the second $9/2^+$ state lies just above the first $9/2^+$ state with the difference being 151 (63) keV for the shell model (experimental) case, (iii) the $21/2_2^+$ state in the dipole band is located above the first $25/2^+$ state with the difference being 104 (149) keV for the shell model (experimental) case, and, (iv) the position of the $11/2^-$ state agrees with the experimental observation within ~ 80 keV. Table II lists the decomposition of angular momenta for protons and neutrons ($I_\pi \otimes I_\nu$) (with probabilities greater than 10 %) and the corresponding dominant wavefunctions along with their probabilities for the positive-parity $g_{7/2}$, $d_{5/2}$ and dipole bands; and the two negative-parity bands due to proton and neutron hole in $h_{11/2}$ orbital.

As it is evident from the wavefunctions in Table II, the positive-parity $g_{7/2}$ band is mainly based on three proton particles in $g_{7/2}$ and two proton particles in $d_{5/2}$ orbital. In addition, there are two neutron holes in the $d_{3/2}$ and $h_{11/2}$ orbitals. Thus in the ground state, the valence proton particle in $g_{7/2}$ orbital is responsible for the spin $7/2^+$ and the neutron holes are coupled to an angular momentum of 0^+, which has the most dominant decomposition angular momentum probability (57.36 %). As the spin increases, the neutron hole pair in the $h_{11/2}$ orbital aligns completely giving rise to an angular momentum of 10^+ in the $23/2^+$ state with 28.18% decomposition probability. For the case of positive-parity $d_{5/2}$ band, there is one proton particle in $d_{5/2}$ orbital and four proton particles in $g_{7/2}$ orbital. Similar to the $g_{7/2}$ band, here there are two neutron holes in the $d_{3/2}$ and $h_{11/2}$ orbitals. The valence proton particle in $d_{5/2}$ orbital is responsible for the spin $5/2^+$ for the lowest state of this band and the neutron holes are coupled to an angular momentum of 0^+, which has the most dominant decomposition probability (51.06 %). Again, as the spin increases, the neutron hole pair in the $h_{11/2}$ orbital breaks giving rise to an angular momentum of 10^+ in the $21/2^+$ state with 42.64% probability. The $25/2^+$ state, however, has a 44.58% (19.63%) angular momentum decomposition probability from protons coupled to $7/2^+$ ($5/2^+$) and neutrons coupled to 10^+. In the case of the dipole band, the $21/2_2^+$ state has a proton configuration $g_{7/2}^3 d_{5/2}^2$ but for the higher spins this changes to $g_{7/2}^4 d_{5/2}^1$, indicating that the valence proton lies mostly in $d_{5/2}$ orbital. Here also, the dominant neutron configuration is $d_{3/2}^{-2} h_{11/2}^{-2}$. But for the excited states in the dipole band, the neutron pair in the $h_{11/2}$ orbital is completely aligned with probabilities 17.93% ($21/2_2^+$),

TABLE II. Decomposition of angular momenta of protons and neutrons (with probabilities greater than 10%) and the corresponding dominant partition of wave-functions for the positive-parity $g_{7/2}$, $d_{5/2}$, dipole bands; and the two negative-parity bands, due to proton and neutron hole in $h_{11/2}$ orbital, in ^{133}Cs using the *jj55pna* interaction.

I	$I_\pi \otimes I_\nu$ (Probability)	Wavefunction (Probability)
$7/2^+$	$7/2_\pi^+ \otimes 0_\nu^+$ (57.36)	$(g_{7/2}^3 d_{5/2}^2)_\pi \otimes (d_{3/2}^{-2} h_{11/2}^{-2})_\nu$ (21.67)
	$5/2_\pi^+ \otimes 4_\nu^+$ (14.03)	$(g_{7/2}^3 d_{5/2}^2)_\pi \otimes (d_{3/2}^{-2} h_{11/2}^{-2})_\nu$ (4.93)
$11/2^+$	$7/2_\pi^+ \otimes 2_\nu^+$ (38.40)	$(g_{7/2}^3 d_{5/2}^2)_\pi \otimes (d_{3/2}^{-2} h_{11/2}^{-2})_\nu$ (15.34)
	$11/2_\pi^+ \otimes 0_\nu^+$ (29.07)	$(g_{7/2}^3 d_{5/2}^2)_\pi \otimes (d_{3/2}^{-2} h_{11/2}^{-2})_\nu$ (12.30)
$15/2^+$	$11/2_\pi^+ \otimes 2_\nu^+$ (30.72)	$(g_{7/2}^3 d_{5/2}^2)_\pi \otimes (d_{3/2}^{-2} h_{11/2}^{-2})_\nu$ (14.28)
	$15/2_\pi^+ \otimes 0_\nu^+$ (21.64)	$(g_{7/2}^3 d_{5/2}^2)_\pi \otimes (d_{3/2}^{-2} h_{11/2}^{-2})_\nu$ (11.81)
	$7/2_\pi^+ \otimes 4_\nu^+$ (18.49)	$(g_{7/2}^3 d_{5/2}^2)_\pi \otimes (d_{3/2}^{-2} h_{11/2}^{-2})_\nu$ (7.86)
$19/2^+$	$7/2_\pi^+ \otimes 6_\nu^+$ (18.89)	$(g_{7/2}^3 d_{5/2}^2)_\pi \otimes (d_{3/2}^{-2} h_{11/2}^{-2})_\nu$ (8.97)
	$11/2_\pi^+ \otimes 4_\nu^+$ (16.46)	$(g_{7/2}^3 d_{5/2}^2)_\pi \otimes (d_{3/2}^{-2} h_{11/2}^{-2})_\nu$ (8.04)
	$5/2_\pi^+ \otimes 8_\nu^+$ (10.77)	$(g_{7/2}^3 d_{5/2}^2)_\pi \otimes (d_{3/2}^{-2} h_{11/2}^{-2})_\nu$ (5.63)
	$15/2_\pi^+ \otimes 2_\nu^+$ (10.00)	$(g_{7/2}^3 d_{5/2}^2)_\pi \otimes (d_{3/2}^{-2} h_{11/2}^{-2})_\nu$ (5.43)
$23/2^+$	$7/2_\pi^+ \otimes 10_\nu^+$ (28.18)	$(g_{7/2}^3 d_{5/2}^2)_\pi \otimes (d_{3/2}^{-2} h_{11/2}^{-2})_\nu$ (14.34)
	$5/2_\pi^+ \otimes 10_\nu^+$ (20.50)	$(g_{7/2}^3 d_{5/2}^2)_\pi \otimes (d_{3/2}^{-2} h_{11/2}^{-2})_\nu$ (9.74)
$5/2^+$	$5/2_\pi^+ \otimes 0_\nu^+$ (51.06)	$(g_{7/2}^4 d_{5/2}^1)_\pi \otimes (d_{3/2}^{-2} h_{11/2}^{-2})_\nu$ (29.99)
	$5/2_\pi^+ \otimes 2_\nu^+$ (15.49)	$(g_{7/2}^4 d_{5/2}^1)_\pi \otimes (d_{3/2}^{-2} h_{11/2}^{-2})_\nu$ (9.34)
$9/2^+$	$5/2_\pi^+ \otimes 2_\nu^+$ (31.40)	$(g_{7/2}^4 d_{5/2}^1)_\pi \otimes (d_{3/2}^{-2} h_{11/2}^{-2})_\nu$ (16.54)
	$9/2_\pi^+ \otimes 0_\nu^+$ (29.69)	$(g_{7/2}^4 d_{5/2}^1)_\pi \otimes (d_{3/2}^{-2} h_{11/2}^{-2})_\nu$ (16.25)
$13/2^+$	$13/2_\pi^+ \otimes 0_\nu^+$ (29.28)	$(g_{7/2}^4 d_{5/2}^1)_\pi \otimes (d_{3/2}^{-2} h_{11/2}^{-2})_\nu$ (19.71)
	$9/2_\pi^+ \otimes 2_\nu^+$ (25.95)	$(g_{7/2}^4 d_{5/2}^1)_\pi \otimes (d_{3/2}^{-2} h_{11/2}^{-2})_\nu$ (13.67)
	$5/2_\pi^+ \otimes 4_\nu^+$ (10.37)	$(g_{7/2}^4 d_{5/2}^1)_\pi \otimes (d_{3/2}^{-2} h_{11/2}^{-2})_\nu$ (4.72)
	$13/2_\pi^+ \otimes 2_\nu^+$ (10.23)	$(g_{7/2}^4 d_{5/2}^1)_\pi \otimes (d_{3/2}^{-2} h_{11/2}^{-2})_\nu$ (6.57)
$17/2^+$	$17/2_\pi^+ \otimes 0_\nu^+$ (39.41)	$(g_{7/2}^4 d_{5/2}^1)_\pi \otimes (d_{3/2}^{-2} h_{11/2}^{-2})_\nu$ (29.54)
	$13/2_\pi^+ \otimes 2_\nu^+$ (22.52)	$(g_{7/2}^4 d_{5/2}^1)_\pi \otimes (d_{3/2}^{-2} h_{11/2}^{-2})_\nu$ (12.53)
$21/2^+$	$5/2_\pi^+ \otimes 10_\nu^+$ (42.64)	$(g_{7/2}^4 d_{5/2}^1)_\pi \otimes (d_{3/2}^{-2} h_{11/2}^{-2})_\nu$ (23.98)
$25/2^+$	$7/2_\pi^+ \otimes 10_\nu^+$ (44.58)	$(g_{7/2}^3 d_{5/2}^2)_\pi \otimes (d_{3/2}^{-2} h_{11/2}^{-2})_\nu$ (18.04)
	$5/2_\pi^+ \otimes 10_\nu^+$ (19.63)	$(g_{7/2}^5)_\pi \otimes (d_{3/2}^{-2} h_{11/2}^{-2})_\nu$ (5.65)
$21/2_2^+$	$7/2_\pi^+ \otimes 8_\nu^+$ (25.74)	$(g_{7/2}^3 d_{5/2}^2)_\pi \otimes (d_{3/2}^{-2} h_{11/2}^{-2})_\nu$ (10.52)
	$7/2_\pi^+ \otimes 10_\nu^+$ (17.93)	$(g_{7/2}^3 d_{5/2}^2)_\pi \otimes (d_{3/2}^{-2} h_{11/2}^{-2})_\nu$ (7.58)
	$5/2_\pi^+ \otimes 8_\nu^+$ (10.01)	$(g_{7/2}^3 d_{5/2}^2)_\pi \otimes (d_{3/2}^{-2} h_{11/2}^{-2})_\nu$ (3.62)
$23/2_2^+$	$5/2_\pi^+ \otimes 10_\nu^+$ (43.96)	$(g_{7/2}^4 d_{5/2}^1)_\pi \otimes (d_{3/2}^{-2} h_{11/2}^{-2})_\nu$ (22.90)
	$9/2_\pi^+ \otimes 10_\nu^+$ (11.54)	$(g_{7/2}^4 d_{5/2}^1)_\pi \otimes (d_{3/2}^{-2} h_{11/2}^{-2})_\nu$ (5.79)
$25/2_2^+$	$5/2_\pi^+ \otimes 10_\nu^+$ (22.91)	$(g_{7/2}^4 d_{5/2}^1)_\pi \otimes (d_{3/2}^{-2} h_{11/2}^{-2})_\nu$ (11.13)
	$5/2_\pi^+ \otimes 12_\nu^+$ (22.87)	$(g_{7/2}^4 d_{5/2}^1)_\pi \otimes (d_{3/2}^{-1} s_{1/2}^{-1} h_{11/2}^{-2})_\nu$ (14.89)
	$7/2_\pi^+ \otimes 10_\nu^+$ (16.52)	$(g_{7/2}^4 d_{5/2}^1)_\pi \otimes (d_{3/2}^{-2} h_{11/2}^{-2})_\nu$ (9.14)
$27/2_2^+$	$5/2_\pi^+ \otimes 12_\nu^+$ (21.38)	$(g_{7/2}^4 d_{5/2}^1)_\pi \otimes (d_{3/2}^{-2} s_{1/2}^{-1} h_{11/2}^{-2})_\nu$ (11.66)
	$7/2_\pi^+ \otimes 10_\nu^+$ (18.81)	$(g_{7/2}^5)_\pi \otimes (d_{3/2}^{-2} h_{11/2}^{-2})_\nu$ (5.14)
$29/2_2^+$	$9/2_\pi^+ \otimes 10_\nu^+$ (18.99)	$(g_{7/2}^4 d_{5/2}^1)_\pi \otimes (d_{3/2}^{-2} h_{11/2}^{-2})_\nu$ (10.76)
	$5/2_\pi^+ \otimes 12_\nu^+$ (18.32)	$(g_{7/2}^4 d_{5/2}^1)_\pi \otimes (d_{3/2}^{-1} s_{1/2}^{-1} h_{11/2}^{-2})_\nu$ (7.23)
	$7/2_\pi^+ \otimes 12_\nu^+$ (15.43)	$(g_{7/2}^4 d_{5/2}^1)_\pi \otimes (d_{3/2}^{-1} s_{1/2}^{-1} h_{11/2}^{-2})_\nu$ (7.28)
$31/2_2^+$	$11/2_\pi^+ \otimes 10_\nu^+$ (21.38)	$(g_{7/2}^4 d_{5/2}^1)_\pi \otimes (d_{3/2}^{-2} h_{11/2}^{-2})_\nu$ (13.77)
	$13/2_\pi^+ \otimes 10_\nu^+$ (19.04)	$(g_{7/2}^4 d_{5/2}^1)_\pi \otimes (d_{3/2}^{-2} h_{11/2}^{-2})_\nu$ (12.97)
	$7/2_\pi^+ \otimes 12_\nu^+$ (15.12)	$(g_{7/2}^5)_\pi \otimes (d_{3/2}^{-1} s_{1/2}^{-1} h_{11/2}^{-2})_\nu$ (4.88)
$33/2_2^+$	$13/2_\pi^+ \otimes 10_\nu^+$ (25.39)	$(g_{7/2}^4 d_{5/2}^1)_\pi \otimes (d_{3/2}^{-2} h_{11/2}^{-2})_\nu$ (15.64)
	$17/2_\pi^+ \otimes 10_\nu^+$ (24.09)	$(g_{7/2}^4 d_{5/2}^1)_\pi \otimes (d_{3/2}^{-2} h_{11/2}^{-2})_\nu$ (17.64)
	$15/2_\pi^+ \otimes 10_\nu^+$ (12.82)	$(g_{7/2}^4 d_{5/2}^1)_\pi \otimes (d_{3/2}^{-2} h_{11/2}^{-2})_\nu$ (7.14)
$11/2^-$	$11/2_\pi^- \otimes 0_\nu^+$ (47.28)	$(g_{7/2}^4 h_{11/2}^1)_\pi \otimes (d_{3/2}^{-2} h_{11/2}^{-2})_\nu$ (26.57)
	$11/2_\pi^- \otimes 2_\nu^+$ (27.93)	$(g_{7/2}^4 h_{11/2}^1)_\pi \otimes (d_{3/2}^{-2} h_{11/2}^{-2})_\nu$ (15.28)
$15/2^-$	$11/2_\pi^- \otimes 2_\nu^+$ (34.01)	$(g_{7/2}^4 h_{11/2}^1)_\pi \otimes (d_{3/2}^{-2} h_{11/2}^{-2})_\nu$ (17.86)
	$15/2_\pi^- \otimes 0_\nu^+$ (24.95)	$(g_{7/2}^4 h_{11/2}^1)_\pi \otimes (d_{3/2}^{-2} h_{11/2}^{-2})_\nu$ (12.69)
	$15/2_\pi^- \otimes 2_\nu^+$ (11.53)	$(g_{7/2}^4 h_{11/2}^1)_\pi \otimes (d_{3/2}^{-2} h_{11/2}^{-2})_\nu$ (4.78)
$19/2^-$	$19/2_\pi^- \otimes 0_\nu^+$ (34.60)	$(g_{7/2}^4 h_{11/2}^1)_\pi \otimes (d_{3/2}^{-2} h_{11/2}^{-2})_\nu$ (22.43)
	$19/2_\pi^- \otimes 2_\nu^+$ (24.49)	$(g_{7/2}^4 h_{11/2}^1)_\pi \otimes (d_{3/2}^{-2} h_{11/2}^{-2})_\nu$ (14.94)
	$15/2_\pi^- \otimes 2_\nu^+$ (17.72)	$(g_{7/2}^4 h_{11/2}^1)_\pi \otimes (d_{3/2}^{-2} h_{11/2}^{-2})_\nu$ (9.36)
$23/2^-$	$23/2_\pi^- \otimes 0_\nu^+$ (34.17)	$(g_{7/2}^3 d_{5/2}^1 h_{11/2}^1)_\pi \otimes (d_{3/2}^{-2} h_{11/2}^{-2})_\nu$ (13.85)
	$23/2_\pi^- \otimes 2_\nu^+$ (17.58)	$(g_{7/2}^3 d_{5/2}^1 h_{11/2}^1)_\pi \otimes (d_{3/2}^{-2} h_{11/2}^{-2})_\nu$ (8.01)
	$19/2_\pi^- \otimes 2_\nu^+$ (13.44)	$(g_{7/2}^4 h_{11/2}^1)_\pi \otimes (d_{3/2}^{-2} h_{11/2}^{-2})_\nu$ (5.43)
$15/2_2^-$	$7/2_\pi^+ \otimes 5_\nu^-$ (40.58)	$(g_{7/2}^5)_\pi \otimes (d_{3/2}^{-2} s_{1/2}^{-1} h_{11/2}^{-1})_\nu$ (15.94)
	$5/2_\pi^+ \otimes 5_\nu^-$ (24.16)	$(g_{7/2}^5)_\pi \otimes (d_{3/2}^{-2} s_{1/2}^{-1} h_{11/2}^{-1})_\nu$ (11.10)
$19/2_2^-$	$7/2_\pi^+ \otimes 7_\nu^-$ (44.75)	$(g_{7/2}^5)_\pi \otimes (d_{3/2}^{-1} h_{11/2}^{-1})_\nu$ (16.53)
	$5/2_\pi^+ \otimes 7_\nu^-$ (24.91)	$(g_{7/2}^5)_\pi \otimes (d_{3/2}^{-1} h_{11/2}^{-1})_\nu$ (10.92)
$21/2_2^-$	$7/2_\pi^+ \otimes 7_\nu^-$ (53.56)	$(g_{7/2}^5)_\pi \otimes (d_{3/2}^{-1} h_{11/2}^{-1})_\nu$ (22.24)

FIG. 6. (Color online) Comparison between experiment and shell model calculations for the positive-parity yrast, dipole, and negative-parity bands in ^{133}Cs.

43.96% $(23/2_2^+)$, 22.91% $(25/2_2^+)$, 18.81 $(27/2_2^+)$ showing that the shell model agrees with the three-quasiparticle nature of this dipole band. In addition, for the $25/2_2^+$ and $27/2_2^+$ states, there are contributions from the neutron configuration $d_{3/2}^{-1}s_{1/2}^{-1}h_{11/2}^{-2}$, giving a neutron angular momentum coupling of 12^+. For the remaining higher spin states $(29/2_2^+$ to $33/2_2^+)$, the proton-particle pair in $g_{7/2}$ breaks giving rise to dominant proton angular momentum coupling of $9/2^+$ (18.99%), $11/2^+$ (21.38%), and $13/2^+$ (25.39%) respectively.

The negative-parity bands as shown in Table II, have two different origins: (i) due to the presence of a proton particle in the $h_{11/2}$ orbital $(\pi g_{7/2}^4 h_{11/2}^1)$ and (ii) due to a neutron hole in the $s_{1/2}$ or $d_{3/2}$ and $h_{11/2}$ orbital $(\nu d_{3/2}^{-2}s_{1/2}^{-1}h_{11/2}^{-1}$ or $\nu d_{3/2}^{-1}h_{11/2}^{-1})$. Bands arising from these two structures have been observed in the present experiment. Similar bands have also been observed in ^{135}La as given in Refs. [34, 35]. The first set of negative-parity bands $(11/2^-, 15/2^-, 19/2^-,$ and $23/2^-)$ have a dominant wavefunction with four proton particles in the $g_{7/2}$ orbital and one proton particle in the $h_{11/2}$ orbital. There are two neutron holes in the $d_{3/2}$ and $h_{11/2}$ orbitals, similar to the case of positive-parity states. The valence

proton particle in $h_{11/2}$ orbital is responsible for the spin $11/2^-$ and the neutron holes are coupled to an angular momentum of 0^+ for the lowest state of this band, which is the most dominant decomposition probability (47.28%). For the $15/2^-$ state, the maximum contribution (34.01%) comes from the decomposition $I_\pi \otimes I_\nu = 11/2_\pi^- \otimes 2_\nu^+$, with additional contribution from a proton pair breaking in $g_{7/2}$ orbital giving rise to $15/2_\pi^-$ and neutrons coupled to 0^+. For the $19/2^-$ and $23/2^-$ states, the governing contributions are from neutrons coupled to 0^+ and protons coupled to $19/2^-$ (34.60%) and $23/2^-$ (34.17%) respectively. The second set of negative-parity states $(15/2_2^-, 19/2_2^-,$ and $21/2_2^-)$ have a dominant wavefunction with all five proton particles in the $g_{7/2}$ orbital and neutron configuration $\nu d_{3/2}^{-2}s_{1/2}^{-1}h_{11/2}^{-1}$ for $15/2_2^-$ and $d_{3/2}^{-1}h_{11/2}^{-1}$ for $19/2_2^-$ and $21/2_2^-$ states. The valence proton particle in $g_{7/2}$ orbital and one neutron hole each in $s_{1/2}$ and $h_{11/2}$ orbital is responsible for the spin $15/2_2^-$ state of this band, which has a maximum decomposition probability (40.58%). The maximum contributions for the $19/2_2^-$ and $21/2_2^-$ states comes from $I_\pi = 7/2^+$ and $I_\nu = 7^-$ with probabilities 44.75% and 53.56%, respec-

$15/2^+_\pi \times 0^+_\nu$ (67.33%)

$(g_{7/2}^4 d_{5/2}^1)_\pi \times (d_{3/2}^{-2})_\nu$
(29.95%)

$11/2^+_\pi \times 2^+_\nu$ (30.72%)

$(g_{7/2}^3 d_{5/2}^2)_\pi \times (d_{3/2}^{-2} h_{11/2}^{-2})_\nu$
(14.28%)

$15/2^+$ 1794

$15/2^+_\pi \times 0^+_\nu$ (100%)

$(g_{7/2}^5)_\pi$ (47.38%)

$15/2^+$ 1660

$15/2^+$ 1435

$7/2^+_\pi \times 2^+_\nu$ (48.04%)

$(g_{7/2}^5)_\pi \times (d_{3/2}^{-2})_\nu$
(23.10%)

$7/2^+_\pi \times 2^+_\nu$ (38.40%)

$(g_{7/2}^3 d_{5/2}^2)_\pi \times (d_{3/2}^{-2} h_{11/2}^{-2})_\nu$
(15.34%)

$11/2^+$ 1268

$11/2^+_\pi \times 0^+_\nu$ (100%)

$(g_{7/2}^5)_\pi$ (51.85%)

$11/2^+$ 890

$11/2^+$ 691

$7/2^+_\pi \times 0^+_\nu$ (57.36%)

$(g_{7/2}^3 d_{5/2}^2)_\pi \times (d_{3/2}^{-2} h_{11/2}^{-2})_\nu$
(21.67%)

$7/2^+_\pi \times 0^+_\nu$ (78.52%)

$(g_{7/2}^5)_\pi \times (d_{3/2}^{-2})_\nu$
(33.58%)

$7/2^+_\pi \times 0^+_\nu$ (100%)

$(g_{7/2}^5)_\pi$ (45.40%)

$7/2^+$ 0

$^{133}Cs_{78}$

$7/2^+$ 0

$^{135}Cs_{80}$
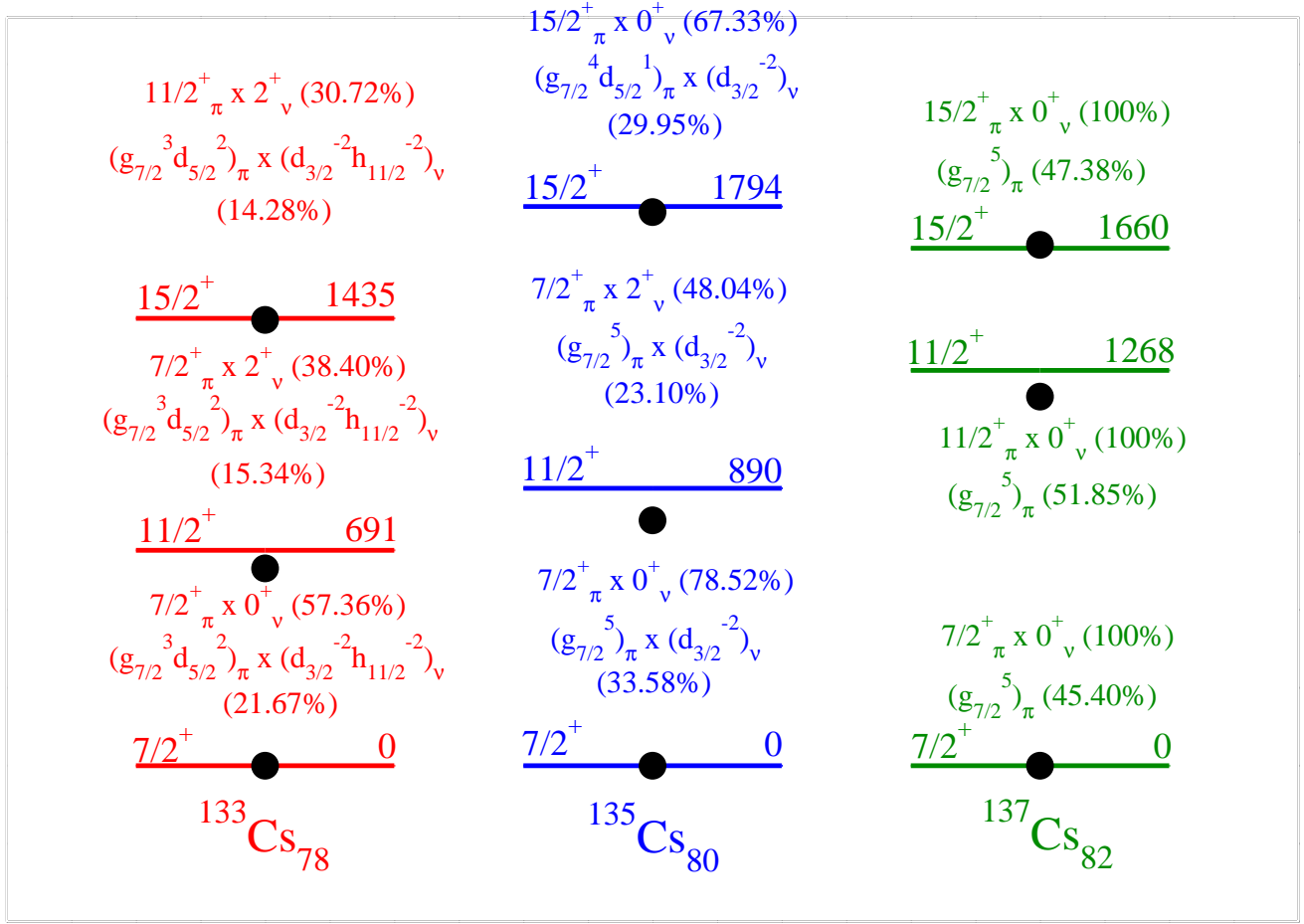
$7/2^+$ 0

$^{137}Cs_{82}$

FIG. 7. (Color online) Comparison between experiment (black filled circles) and shell model calculations for the $7/2^+$, $11/2^+$ and $15/2^+$ states of the positive-parity yrast bands in ^{133,135,137}Cs. There are two expressions for each state: the first expression shows the dominant angular momentum decomposition and the second expression shows the largest wavefunction partition corresponding to the dominant angular momentum decomposition. A detailed explanation of these expressions are given in the text.

tively.

LSSM calculations without truncation for ^{135,137}Cs isotopes when compared with the experimental results give an overall good description of the level structure for the positive as well as negative-parity states [33, 36]. However, some deviation has been observed for the negative parity states with higher spin. Comparison between experiment (black filled circles) and shell model calculations for the $7/2^+$, $11/2^+$ and $15/2^+$ states of the positive-parity yrast bands in ^{133,135,137}Cs have been shown in the Fig. 7. The dominant angular momentum decomposition and the corresponding largest wavefunction partition (the most dominant configuration) have also been shown. For the ground state ($7/2^+$) in ^{137}Cs, the first expression depicts the angular momentum decomposition due to protons (π) and neutrons (ν), respectively: $7/2^+_\pi \times 0^+_\nu$ (100%). The neutrons do not participate in the excitation as the shell is completely filled. The five valence proton particles thus couple to generate an angular momentum of 7/2 and this leads to the angular momentum decomposition probability being 100%. However, this angular momentum decomposition does not convey the exact configuration of the valence proton particles in the different valence orbitals, and hence a knowledge of the wavefunction is required. The wavefunction (configuration) of the $7/2^+$ state corresponding to the angular momentum decomposition $7/2^+_\pi \times 0^+_\nu$ is given in the second expression. The LSSM calculations give the following wavefunction partitions, which add to 96.65% ($< 100\%$): (i) $(g_{7/2}^5)_\pi$ (45.40%), (ii) $(g_{7/2}^3 d_{5/2}^2)_\pi$ (29.89%), (iii) $(g_{7/2}^3 h_{11/2}^2)_\pi$ (11.46%), (iv) $(g_{7/2}^3 d_{3/2}^2)_\pi$ (4.16%), (v) $(g_{7/2}^1 d_{5/2}^2 h_{11/2}^2)_\pi$ (2.23%), (vi) $(g_{7/2}^1 d_{5/2}^4)_\pi$ (1.87%), and (vii) $(g_{7/2}^3 s_{1/2}^2)_\pi$ (1.64%). In Fig. 7, only the most dominant wavefunction partition has been shown.

The angular momentum decomposition for the ground state ($7/2^+$) in ^{135}Cs has also been shown in the first expression: $7/2^+_\pi \times 0^+_\nu$ (78.52%). Here, the neutrons also participate in excitations and hence the angular momentum decomposition probability is not 100% (contrary

to ^{137}Cs). LSSM also gives other decompositions like: $5/2_\pi^+ \times 2_\nu^+$ (7.60%), $11/2_\pi^+ \times 2_\nu^+$ (5.33%), $9/2_\pi^+ \times 2_\nu^+$ (2.87%), $3/2_\pi^+ \times 2_\nu^+$ (2.05%) and $7/2_\pi^+ \times 2_\nu^+$ (1.38%). The sum of all these probabilities gives 97.75% ($< 100\%$). Only the dominant angular momentum decomposition is shown in Fig. 7. The second expression depicts the wavefunction of the $7/2^+$ state corresponding to the dominant angular momentum decomposition, $7/2_\pi^+ \times 0_\nu^+$ (78.52%). Shell model again gives a number of wavefunction partitions: $(g_{7/2}^5)_\pi \times (d_{3/2}^{-2})_\nu$ (33.58%), $(g_{7/2}^3 d_{5/2}^2)_\pi \times (d_{3/2}^{-2})_\nu$ (23.78%), $(g_{7/2}^3 h_{11/2}^2)_\pi \times (d_{3/2}^{-2})_\nu$ (9.48%), etc. The sum of probabilities for all these partitions add to 66.84% ($< 78.52\%$).

The analysis of the wavefunctions indicated that the amplitude of the most dominant configuration for the $15/2^+$ state reduces from 47.38% for ^{137}Cs to 14.28% for ^{133}Cs. This demonstrates the increase in the mixing of configurations when one goes away from N=82 shell gap. Shell model calculations with a truncated model space, i.e., model space consisting of proton $g_{7/2}$, $d_{5/2}$ orbitals and neutron $g_{7/2}$, $d_{5/2}$, $d_{3/2}$, $s_{1/2}$, and $h_{11/2}$ orbitals have also been used to calculate the positive-parity energy levels in $^{129-133}$Cs. However, the energy levels obtained from such calculations are very much compressed. This shows that a full model space is required to explain the excited sates in odd-A Cs isotopes.

V. SUMMARY AND CONCLUSIONS

High-spin states in ^{133}Cs have been studied using the heavy ion induced fusion evaporation reaction ^{130}Te(^{7}Li,4n)^{133}Cs. The new data on the high spin states in ^{133}Cs are important addition to the systematics of odd-A Cs isotopes, i.e., ^{127,129,131,135,137}Cs. Three different band structures, also seen in other odd-A Cs nuclei, viz. bands built on the $7/2^+$, $5/2^+$ and $11/2^-$ states have been identified in ^{133}Cs. The proton $h_{11/2}$ band reported in the present work fits nicely with the systematics. The excitation energy of this band-head is increasing with mass number for odd-A Cs isotopes, making it non-yrast and therefore difficult to observe for heavier odd-A Cs isotopes. The evolution of collectivity for these bands in odd-Cs looks similar to that of their even-even Xe cores. Additionally, a dipole band arising from a three quasiparticle structure has also been observed. Large scale shell model calculations using the $jj55pna$ interaction have been used to compare the experimental levels of ^{133}Cs with the calculated ones. This comparison of the measured levels with the results of the shell model calculations provided a way for the interpretation of the various excited states in ^{133}Cs. The energy levels from the shell model calculations match remarkably well with the experimental data for the two sets of positive and negative-parity states as has been observed for the measured levels in ^{135,137}Cs isotopes. In case of ^{133}Cs, the shell model calculation has been carried out without truncation of the model space. Therefore, the present comparison really tests the predictive power of the interaction used in the calculation. It will be interesting to test the predictive power of the same model for the lighter odd-A Cs isotopes. However, with the present resources it is difficult to perform calculations for the lighter Cs isotopes without truncation. It is important to note that there is scope for improvements of the calculations to understand the observed discrepancies with the measurements for the dipole band which is underestimated. Interestingly, from the analysis of the LSSM wave functions of certain positive parity states in ^{133,135,137}Cs, it has been demonstarted that the mixing of configurations increases when one goes away from N=82 shell gap. It is important to carry out future measurement of lifetimes of excited states and compare the measured transition strengths with the prediction of the shell model calculation to probe the nature of collectivity of these states.

VI. ACKNOWLEDGEMENTS

[1] R. Kumar, D. Mehta, N. Singh, H. Kaur, A. Görgen, S. Chmel, R. P. Singh and S. Murlithar Eur. Phys. J. A **11**, 5 (2001).

[2] E. Grodner, J. Srebrny, A. A. Pasternak, I. Zalewska, T. Morek, Ch. Droste, J. Mierzejewski, M. Kowalczyk, J. Kownacki, M. Kisieliński, et al., Phys. Rev. Lett. **97**, 172501 (2006).

[3] N. Fotiades, J. A. Cizewski, K. Higashiyama, N. Yoshinaga, E. Teruya, R. Krücken, R. M. Clark, P. Fallon, I. Y. Lee, A. O. Machiavelli, et al., Phys. Rev. C **88**, 064315 (2013).

[4] E. Teruya, N. Yoshinaga, K. Higashiyama, and A. Odahara, Phys. Rev. C **92**, 034320 (2015).

[5] P. Möller, A. J. Sierk, R. Bengtsson, H. Sagawa, and T. Ichikawa, Atomic Data and Nuclear Data Tables **98**, 149 (2012).

[6] F. Lidén, B. Cederwall, P. Ahonen, D. W. Banes, B. Fant, J. Gascon, L. Hildingsson, A. Johnson, S. Juutinen, A. Kirwan, et al., Nucl. Phys. A **550**, 365 (1992).

[7] U. Garg, T. P. Sjoreen, and D. B. Fossan, Phys. Rev. C **19**, 217 (1979).

[8] Y. Liang, R. Ma, E. S. Paul, N. Xu, D. B. Fossan, and R. A. Wyss, Phys. Rev. C **42**, 890 (1990).

[9] L. Hildingsson, W. Klamra, Th. Lindblad, F. Lidén, Y. Liang, R. Ma, E. S. Paul, N. Xu, D. B. Fossan, and J. Gascon, Z. Phys. A **340**, 29 (1991).

[10] R. Kumar, Kuljeet Singh, D. Mehta, Nirmal Singh, S. S. Malik, E. S. Paul, A. Görgen, S. Chmel, R. P. Singh and S. Muralithar, Eur. Phys. J. A **24**, 13 (2005).

[11] U. Garg, T. P. Sjoreen, and D. B. Fossan, Phys. Rev. C **19**, 207 (1979).

[12] Peter Alexander and John P. Lau, Nucl. Phys. A **121**, 612 (1968).

[13] S. Törnkvist, L. Hasselgren, S. Ström, J. -E. Thun, and S. Antman, Nucl. Phys. A **142**, 238 (1970).

[14] H. Tan *et al.*, in proceedings of the IEEE Nuclear Science symposium and Medical Imaging Conference (2008NSS/MIC) Dresdan (IEEE, New York, 2009), p. 2471.

[15] R. Palit, S. Saha, J. Sethi, T. Trivedi, S. Sharma, B. S. Naidu, S. Jadhav, R. Donthi, P. B. Chavan, H. Tan *et al.*, Nucl. Instrum. Methods Phys. Res. Sect. A **680**, 90 (2012).

[16] D. C. Radford, Nucl. Instrum. Methods Phys. Res. Sect. A **361**, 297 (1995).

[17] A. Krämer-Flecken, T. Morek, R. M. Lieder, W. Gast, G. Hebbinghaus, H. M. Jäger, and W. Urban , Nucl. Instrum. Methods Phys. Res. Sect. A **275**, 333 (1989).

[18] K. Starosta, T. Morek, Ch. Droste, S. G. Rohoziński, J. Srebrny, A. Wierzchucka, M. Bergström, B. Herskind, E. Melby, T. Czosnyka *et al.*, Nucl. Instrum. Methods Phys. Res. Sect. A **423**, 16 (1999).

[19] R. Palit, H. C. Jain, P. K. Joshi, S. Nagaraj, B. V. T. Rao, S. N. Chintalapudi, and S. S. Ghugre, Pramana **54**, 347 (2000).

[20] Y. Zheng *et al.*, Phys. Rev. C 87, 044328 (2013).

[21] Wang Lie-Lin, Zhu Li-Hua, Lu Jing-Bin, Wu Xiao-Guang, Li Guang-Sheng, Hao Xin, Zheng Yun, He Chuang-Ye, Wang Lei, Li Xue-Qin, *et al.*, Chin. Phys. Lett. **27**, 022101 (2010)

[22] S. Sihotra, R. Palit, Z. Naik, K. Singh, P. K. Joshi, A. Y. Deo, J. Goswamy, S. S. Malik, D. Mehta, C. R. Praharaj *et al.*, Phys. Rev. C. **78**, 034313 (2008).

[23] A. Astier, M.-G. Porquet, Ts. Venkova, D. Verney, Ch. Theisen, G. Duchêne, F. Azaiez, G. Barreau, D. Curien, I. Deloncle *et al.*, Phys. Rev. C **85**, 064316 (2012).

[24] S. Sihotra, K. Singh, S. S. Malik, J. Goswamy, R. Palit, Z. Naik, D. Mehta, N. Singh, R. Kumar, R. P. Singh, and S. Muralithar **79**, 044317 (2009).

[25] B. A. Brown and W.D.M. Rae, Nucl. Data Sheets **120**, 115 (2014).

[26] NuShellX, W.D.M. Rae, http://www.garsington.eclipse.co.uk.

[27] B. A. Brown, N. J. Stone, J. R. Stone, I. S. Towner, and M. Hjorth-Jensen, Phys. Rev. C **71**, 044317 (2005).

[28] R. Machleidt, F. Sammarruca, and Y. Song, Phys. Rev. C **53**, R1483 (1996).

[29] A. Astier, M.-G. Porquet, Ch. Theisen, D. Verney, I. Deloncle, M. Houry, R. Lucas, F. Azaiez, G. Barreau, D. Curien, *et al.*, Phys. Rev. C **85**, 054316 (2012).

[30] Ł. W. Iskra, R. Broda, R. V. F. Janssens, J. Wrzesiński, B. Szpak, C. J. Chiara, M. P. Carpenter, B. Fornal, N. Hoteling, F. G. Kondev, *et al.*, Phys. Rev. C **89**, 044324 (2014).

[31] A. Astier, M.-G. Porquet, Ts. Venkova, Ch. Theisen, G. Duchêne, F. Azaiez, G. Barreau, D. Curien, I. Deloncle, O. Dorvaux, *et al.*, Eur. Phys. J. A **50**, 2 (2014).

[32] S. Biswas, R. Palit, A. Navin, M. Rejmund, A. Bisoi, M. Saha Sarkar, S. Sarkar, S. Bhattacharya, D. C. Biswas, M. Caamaño, *et al.*, Phys. Rev. C **93**, 034324 (2016).

[33] P. C. Srivastava, M. J. Ermamatov and Irving O Morales J. Phys. G: Nucl. Part. Phys. **40**, 035106 (2013).

[34] Ritika Garg, S. Kumar, Mansi Saxena, Savi Goyal, Davindar Siwal, S. Verma, R. Palit, Sudipta Saha, J. Sethi, Sushil K. Sharma, *et al.*, Phys. Rev. C **87**, 034317 (2013).

[35] R. Leguillon, H. Nishibata, Y. Ito, C. M. Petrache, A. Odahara, T. Shimoda, N. Hamatani, K. Tajiri, J. Takatsu, R. Yokoyama, *et al.*, Phys. Rev. C **88**, 044309 (2013).

[36] S. Biswas *et al.* (to be submitted).